Hygroscopicity and Volatility of Biomass Burning Aromatic and Nitroaromatic Compounds

Malsha Amugoda[1], Prakriti Singh[1], Stephanie Salas[1], James F. Davies[1]*

1. Department of Chemistry, University of California Riverside, Riverside, CA, USA.

**Correspondence to: jfdavies@ucr.edu*

Abstract

The microphysical characteristics of aerosol particles produced from biomass burning will influence their evolution and effects in the atmosphere. Aromatic and nitroaromatic species are produced directly or as oxidation products from biomass burning emissions and many have been found in the condensed phase of the aerosol plume. Although these compounds are generally considered to be of low hygroscopicity, the presence of oxygen functionality can give rise to limited interactions with water vapor that can influence the optical properties and phase of particles via water uptake. Here, we report the hygroscopic characteristics of a range of aromatic and nitroaromatic compounds, revealing a wide variation in the extent of hygroscopic growth across molecules with similar chemical functionality, demonstrating the importance of considering specific molecular interactions when predicting both hygroscopic growth and solubility. We show that 4-nitrocatechol, phthalic acid, and all isomers of nitrophenol exhibit reversible interactions with water, while vanillic acid, syringic acid, p-hydroxybenzoic acid, and nitrobenzaldehyde do not exhibit measurable hygroscopic growth in subsaturated RH conditions. Most components measured did not exhibit measurable evaporation over 2-3 hours at 293 K, indicating vapor pressures $<10^{-5}$ Pa, however the structural isomers of nitrophenol showed significant volatility that varied as a function of molecular structure, RH conditions, and particle phase. We report liquid-state vapor pressures derived from evaporation measurements of aqueous particles at high RH and solid-state vapor pressures derived from measurements under dry conditions. Overall, this manuscript provides important physicochemical data regarding the interactions of a range of

biomass burning compounds with water and discusses the implications of these properties for biomass burning aerosol.

Keywords: Hygroscopicity, Volatility, Biomass burning, Brown carbon, Phase state

Synopsis:

The microphysical properties of biomass burning aerosol particles determine their chemical evolution and effects in the atmosphere. This study characterizes the hygroscopicity, phase state and volatility of levitated particles containing common biomass burning constituents.

TOC Figure:

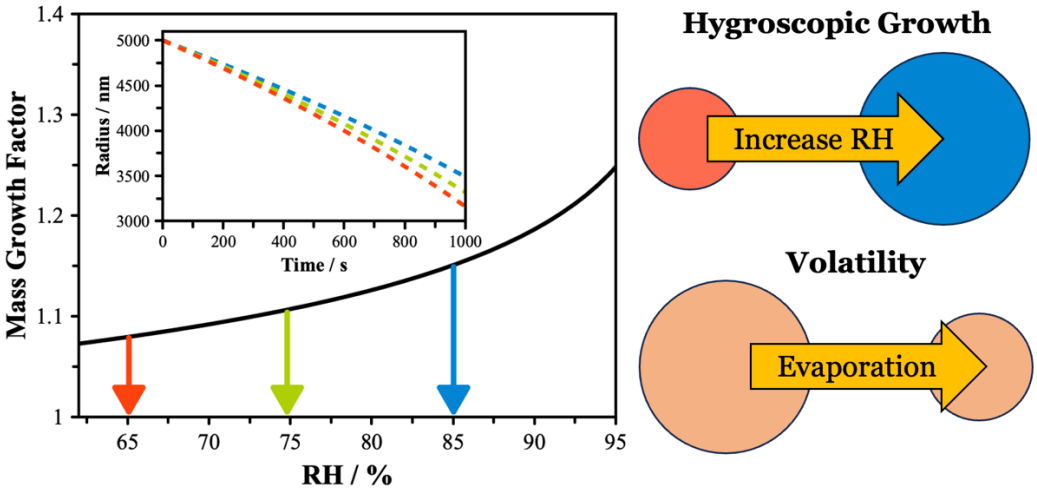

Introduction

Atmospheric aerosols influence the climate of Earth directly, by absorbing or scattering solar radiation,[1,2] and indirectly, by serving as cloud condensation nuclei (CCN) or ice-nucleating particles[3] and altering the cloud optical properties and biogeochemical cycles.[4] A major source of aerosol particles in the atmosphere is biomass burning (BB), which can be broadly categorized as open or quasi-open burning of any non-fossilized vegetative or organic fuel.[5] BB aerosol have created many negative impacts on air quality, human health, and visibility at regional and global scale.[6–9] As well as one of the major global emission sources of primary aerosol particles, BB is a major source of reactive trace gases in the atmosphere, such as carbon monoxide (CO), oxides of nitrogen (NOx), methane (CH_4), and other volatile organic compounds, which may lead to the subsequent formation of secondary organic aerosol (SOA).[10]

The chemical composition of particles produced from BB plumes includes black carbon (BC), organic carbon (OC), inorganic salts, and metal oxides.[11–13] BC are soot-like particles that contain graphitic carbon that can absorb a broad region of solar light from ultraviolet (UV) to infrared (IR).[14] OC shows a strong absorbance of UV and IR light but relatively weak absorbance of visible and near-IR light. However, recent studies have identified a subset of OC termed brown carbon (BrC) that is able to absorb strongly at visible wavelengths, typically <450 nm.[14–16] BrC and BrC precursor chemical components include aromatic and highly conjugated molecules, polycyclic aromatics, and nitro-compounds.[11,13] Nitrated phenolic compounds, such as nitrophenols, nitrocatechol, methylnitrophenol, methylnitrocatechol, and dinitrophenol, have been identified in BB events from different regions, including in cloud water samples from eastern China,[13,17] from winter time domestic wood burning in suburban region of London,[18] and from haze episodes in Shanghai.[19] Furthermore, levoglucosan, anhydrosaccharides, and methoxyphenols, which are the pyrolysis products of cellulose, hemicellulose, and lignin, have been detected in wood smoke.[20] According to the vegetation type, pyrolysis of lignin produces fine aerosols enriched in syringic acid, vanillic acid, and p-hydroxybenzoic acid.[21,22]

Based on laboratory and field studies on UV-induced aging of BB smoke, the high concentration of organic trace gases in the BB plume can lead to SOA formation[23] and enhance the organic aerosol mass.[24,25] For instance, in plumes rich in nitrogen oxides, phenolic compounds, a major aromatic precursor gas in wildfires, oxidize to produce nitrophenolic compounds.[14,26] However, the SOA formation in BB fire smoke plumes can be limited by the dilution-driven evaporative loss of semi-volatile compounds into the gas phase,[23,27] controlled by the volatility of individual organic compounds. The volatility of organic compounds in aerosol particles plays an important role in their chemical evolution in the atmosphere.[28] Compounds that become entrained within particles at or near their source can evaporate over time and

experience further chemical reactions in the gas phase, which can subsequently lead to partitioning back to the particle phase due to the reduction in vapor pressure following oxidation.[29] Knowledge of the vapor pressure of individual components in BB aerosol is necessary to predict and understand the lifetime and chemical evolution of BB aerosol in the atmosphere. Chemical processes occurring within the particles, such as those initiation by heterogeneous reactions with gas-phase oxidants or acid/base reactions, can also lead to changes in volatility through oligomerization and/or the formation of organic salts.[30,31] The importance of particle phase chemistry depends on the relative rate of evaporation versus reaction rates, which can depend strongly on other factors, such as the particle phase.[32,33] The volatility may also depend on the hygroscopic properties of components in the particle phase, as water will control the phase state and chemical activity of semi-volatile components.

Analysis of the hygroscopic response of BB aerosol particles is important for accurate prediction of their effects on climate, air quality, and human health.[34,35] Hygroscopic organic compounds typically contain oxygen functional groups that form hydrogen bonds with water and allow uptake to occur from the gas phase. The oxygen-to-carbon ratio (O/C) of the molecular constituents is generally considered as an indicator of the hygroscopicity, although there is a significant variability of the hygroscopicity parameter (κ in the κ-Köhler framework) even at the same O/C due to the different kinds of molecular interactions possible between different functional groups.[36] The effects of O/C, bulk solubility, functional groups, carbon chain length, and branching of the chemical structure on hygroscopicity of atmospherically relevant carboxylic acids, alcohols, sugars have been studied.[34,36–38] Studies of the hygroscopicity of BB aerosol produced directly from combustion have shown relatively high hygroscopicity that varies with burn conditions and fuel source,[39] while photoxidized phenolic compounds have been shown to exhibit similar hygroscopicity despite different precursors.[40] Elucidating the role of individual components on the hygroscopicity of these chemically complex samples is challenging due to the limited number of studies that have measured the hygroscopicity of water soluble BB aerosol. Furthermore, the volatility of BB compounds will play a significant role in their contribution to aerosol mass, hygroscopicity, and their lifetime in the atmosphere. Hygroscopicity and volatility are connected, with the latter dependent on the chemical activity and phase states of the particles, which both depend on the hygroscopicity.

In this work, we focus on characterizing the hygroscopic growth, solubility, phase and vapor pressures of a series of biomass burning tracer compounds. These compounds include the substituted aromatics vanillic acid, syringic acid, p-hydroxy-benzoic acid, and phthalic acid, and nitroaromatics, including 4-nitrocatechol, 2, 3 and 4-nitrophenol, nitrobenzaldehyde and nitrobenzoic acid. These compounds are commonly found in biomass burning aerosol and contribute, either directly or as precursors, to light

absorption in BrC aerosol. Although these compounds do not exist in isolation in atmospheric aerosol, characterizing their physical properties in single component particles allows for informed estimates of their properties in mixtures. Our aim is to provide a complete set of physicochemical data for these compounds, supporting future studies and allowing an improved interpretation of the role of these compounds on ambient particle properties. Furthermore, this work serves to demonstrate how minor changes in the molecular structure or functional groups can lead to significant changes in the physical characteristics of the particles.

Methods

Sample Preparation

All chemicals used in this study were purchased and utilized without additional purification. Hygroscopic growth measurements were conducted using particles containing 4-nitrophenol (4NP, Sigma Aldrich, ≥ 99.0% purity), 3-nitrophenol (3NP, Sigma Aldrich, 99.0% purity), 2-nitrophenol (2NP, Sigma Aldrich, 98.0% purity), 4-nitrocatechol (4NC, Sigma Aldrich, 97.0% purity), 2-nitrobenzaldehyde (ACROS Organics, 99+%), 4-nitrobenzoic acid (Sigma Aldrich, 98.0% purity), syringic acid (Sigma Aldrich, ≥ 95.0% purity), vanillic acid (Sigma Aldrich, 97.0% purity), p-hydroxybenzoic acid (Sigma Aldrich, 99.0% purity), and phthalic acid (Sigma Aldrich, ≥ 99.5% purity). Pure component solutions were prepared in a concentration range of 5 - 20 g/L with a 1:1 mixture of isopropanol (Fisher Chemical, HPLC grade) and HPLC water (Fisher Chemical). The solutions were stored in a pre-cleaned glass vials and stored in dark conditions to prevent their interaction with light. RH probe calibrations were done using potassium carbonate (Fisher Chemical, >99% purity), potassium chloride (Sigma Aldrich, >99.0 purity), sodium chloride (Fisher Chemical, >99% purity), and lithium chloride (Sigma Aldrich, 99.0% purity).

Particle Levitation

A linear quadrupole electrodynamic balance (LQ-EDB) was used to levitate individual particles, as described in detail in our previously published work.[35,41] Briefly, a droplet dispenser (MicroFab MJ-ABP-01, 30 μm orifice), positioned in front of an induction electrode at 180 to 200V, is loaded with ~12 μL of sample solution and a single charged droplet is produced by application of a voltage pulse and introduced into the LQ-EDB chamber. The charged droplet initially travels horizontally to the center of the four electrode rods and falls under gravity along the axis of the trap confined by the electric field established due to paired out-of-phase AC voltages applied to the quadrupole. A 532 nm laser was used to illuminate the droplet to visually verify trapping. In addition to the gravitational force, the presence of gas flow in the LQ-EDB exerts a drag force on the droplet, and these two forces are balanced by a repulsive electrostatic force created by a DC voltage applied to the disk electrode in the center of the LQ-EDB. A CMOS camera

was used to visualize the droplet and stabilize the position of the droplet by changing the DC voltage through PID feedback loop using LabVIEW software. The gas flow to the LQ-EDB consisting of dry and humidified nitrogen at a total flow rate of 180 sccm was used to control the RH of the chamber. The RH in the chamber was monitored using a RH probe, which was calibrated using the deliquescence RH of NaCl, K_2CO_3, KCl, and LiCl. Following initial trapping, the droplet loses excess water and reaches an equilibrium composition with the gas phase RH - at this point, we refer to the sample as a particle. For spherical particles, Mie resonance spectroscopy (see Supporting Information) was used to probe the evolving size of the sample. For solid particles that were non-spherical, spectroscopic methods failed and we applied mass spectrometry (see Supporting Information) and electrostatic analysis to characterize the relative mass of the particle.

Electrostatic Analysis

Under static gas conditions, the DC voltage to balance the particle is directly proportional to the mass of the particle, with the assumption that the charge on the droplet is constant, according to:

$$mg = \frac{CqV'}{2z} \qquad (1)$$

where m is the mass of the particle, g is the gravitational acceleration, C is a geometrical constant, q is the particle charge, and V' is the DC voltage, and z is the height of the particle above the electrode. In static gas conditions, the absence of a gas flow makes the RH in the chamber hard to control. Thus, we devised a method to manipulate the gas flows in the chamber in a manner that allowed both rigorous gas phase control as well as the ability to characterize the relative mass. To measure the mass-based hygroscopicity of the pure compounds of interest, a single particle was levitated at a fixed RH in the presence of a gas flow. To measure the DC voltage under static conditions (V' – note that the "prime" indicates a voltage measured without a gas flow), the gas flow was temporarily diverted using a pneumatic valve operated in an automated sequence. With the change in gas flow, the particle moved to a new position in the trap and the DC voltage was automatically switched and varied to rebalance to the original position and ensure a constant height (z). The gas flow was then reintroduced and the original DC voltage necessary to balance the particle in the flow (V) was restored. This sequence was repeated several times to stabilize the particle under flow-on and flow-off conditions, verified by the extent of variation in the DC voltage required to balance the particle. The sequence was then repeated several more times to measure the DC voltage required to balance the droplet in both sets of flow conditions. The RH was then varied in 5% increments, in the range 0 to ~95%, and the DC balancing voltage was recorded at each step as described. The flow-off DC balancing voltage at 0% RH is proportional to the dry mass of the particle, allowing the mass growth factor at each RH to be calculated according to:

$$m(RH)/m_0 = V'(RH)/V_0' \qquad (2)$$

This method was validated against NaCl and ammonium sulfate particles, as discussed in the Supporting Information.

Evaporation Model

The evaporation rate of the organic component from a spherical particle is dependent on both its vapor pressure and hygroscopicity. For a single component spherical particle containing a semi-volatile organic compound undergoing isothermal evaporation in the continuum regime, the evaporation rate is given by:

$$\frac{da^2}{dt} = \frac{2M_{org}D_{org}}{\rho_a RT} p_{eff} \qquad (3)$$

where a is the particle radius, M_{org} is the molar mass of the organic, D_{org} is the gas phase diffusion coefficient, ρ_a is the density of the particle, and p_{eff} is the effective vapor pressure of the organic. For organic particles that coexist in equilibrium with water, the evaporation rate is modified based on how much water is associated with each evaporating organic molecule. To account for this, we introduce a correction factor that equals the mass ratio of water to the mass of organic, giving the equation:

$$\frac{da^2}{dt} = \frac{2M_{org}D_{org}}{\rho_a RT} p_{org}\gamma_{org}x_{org} \times \left[\frac{(1-x_{org})M_w}{x_{org}M_{org}} + 1\right] \qquad (4)$$

where the effective vapor pressure has been replaced by the product of the pure component vapor pressure (p_{org}), activity coefficient (γ_{org}) and mole fraction (x_{org}), and the square bracket is a correction factor to based on the mass ratio of water to organic, allowing the evaporation rate to account for the co-evaporation of water, introduced in our earlier work.[42] These equations predict a linear dependence of the radius-squared on time, and the evaporation rate is quoted as the slope of this function.

Results and Discussion

We break down the results over the subsequent subsections according to the general class of molecules studied. In each section we discuss the behavior of levitated particles consisting of each compound, reporting on their response to changes in RH and their evolution over time. Table 1 summarizes the physical properties and molecular structures of the compounds, including data from this work and literature sources, where available.

Table 1: Physical and chemical properties of the compounds explored in this study. Values derived from measurements reported herein are in bold.

Compound	Molecular weight / g mol^{-1}	O/C	Density / g mL^{-1}	Solubility / g L^{-1}	Vapor pressure (solid-state) / Pa at 298 K	Vapor pressure (liquid-state) / Pa at 298K

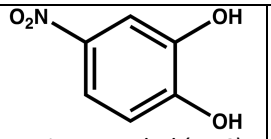 *4-Nitrocatechol (4NC)*	155.11	0.67	1.6 ± 0.1[a]	**12.2**[b]	4.13 ± 0.62 × 10^{-5} [c]	9.99 ± 4.99 × 10^{-4} [c]
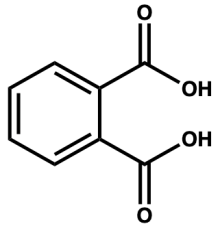 *Phthalic acid (PA)*	166.13	0.5	1.59	**6**[b]	1.77 ± 0.27 × 10^{-5} [c]	1.68 ± 0.84 × 10^{-3} [c]
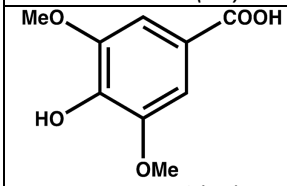 *Syringic acid (SA)*	198.17	0.56	1.34 ± 0.06[a]	2.3[d]	3.37 ± 0.50 × 10^{-5} [c]	9.80 ± 4.90 × 10^{-4} [c]
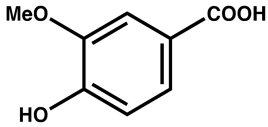 *Vanillic acid (VA)*	168.15	0.50	1.35 ± 0.06 [a]	1.3[e]	6.50 ± 0.98 × 10^{-5} [c]	1.42 ± 0.71 × 10^{-3} [c]
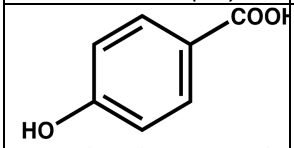 *p-Hydroxybenzoic acid (pHBA)*	138.12	0.43	1.46 [a]	6.1[f]	2.29 × 10^{-5} [c]	8.11 × 10^{-4} [c]
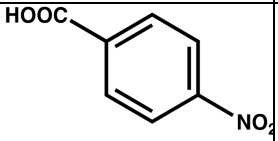 *4-Nitrobenzoic acid (4NBA)*	167.12	0.57	1.61 [a]	**<1**[b]		3.37 x 10^{-4} [i]
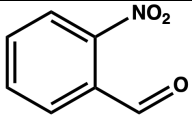 *2-Nitrobenzaldehyde (2NB)*	151.12	0.43	1.34 ± 0.06 [a]	**<1**[b]	3.32 × 10^{-2} [k]	2.15 [k]
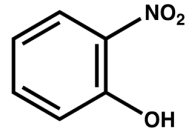 *2-Nitrophenol (2NP)*	139.11	0.5	1.50 [a]	**2-3**[b] <1 [g]	8.94 × 10^{-4} [k]	1.38 × 10^{-3} [k] **3.5 x 10^{-1}** [b]
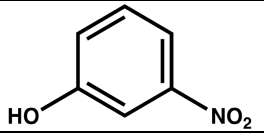	139.11	0.5	1.28 [a]	**10.7**[b]	7.8 x 10^{-3} [i]	1.14 x 10^{-2} [i] **3.6 x 10^{-2}** [b]

3-Nitrophenol (3NP)						**5.0 x 10^{-2}** [b]
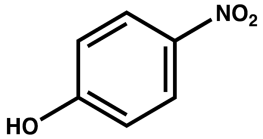 *4-Nitrophenol (4NP)*	139.11	0.5	1.5 [a]	**10.4**[b] 11.6[g]	1.31 × 10^{-2} [h] 1.6 × 10^{-3} [i] **4.7 x 10^{-3}** [b]	1.11 x 10^{-1} [h] 5.14 × 10^{-3} [i] **1.0 x 10^{-2}** [b]

[a] https://scifinder-n.cas.org/
[b] Solubilities and vapor pressure were measured at approximately 293 K in this study
[c] Booth et al.[43] (estimated liquid-state vapor pressures reported)
[d] Queimada et al.[44]
[e] Vilas-Boas et al.[45] (solubility at 298.2 K)
[f] Gracin et al.[46] (solubility at 298.2 K)
[g] https://pubchem.ncbi.nlm.nih.gov/compound/6947#section=Solubility
[h] Schwarzenbach et al.[47] (vapor pressure of liquid at 293.15 K) (overestimated values)
[i] Bannan et al.[48] (±75% estimated error for liquid-state vapor pressure) (<40% error for solid-state vapor pressure)
[j] https://pubchem.ncbi.nlm.nih.gov/source/hsdb/1133
[k] Shelley et al.[49]
[l] https://pubchem.ncbi.nlm.nih.gov/source/hsdb/2140#section=Vapor-Pressure

4-Nitrocatechol and Phthalic Acid

The two most hygroscopic compounds explored in this study were 4-nitrocatechol (4NC) and phthalic acid (PA). Our previous work showed that 4-nitrocatechol particles are aqueous at high RH and experience measurable water uptake in sub-saturated RH conditions.[35] Hygroscopicity was reported using radial growth factors, which are useful for predicting the cloud forming potential, as they allow κ to be directly calculated. Particle efflorescence was observed in the range 50 to 70% RH. Here, we additionally report the hygroscopic growth using mass growth factors, which are typically more useful when the concentration of solutes is required, for example in estimating reaction rates.

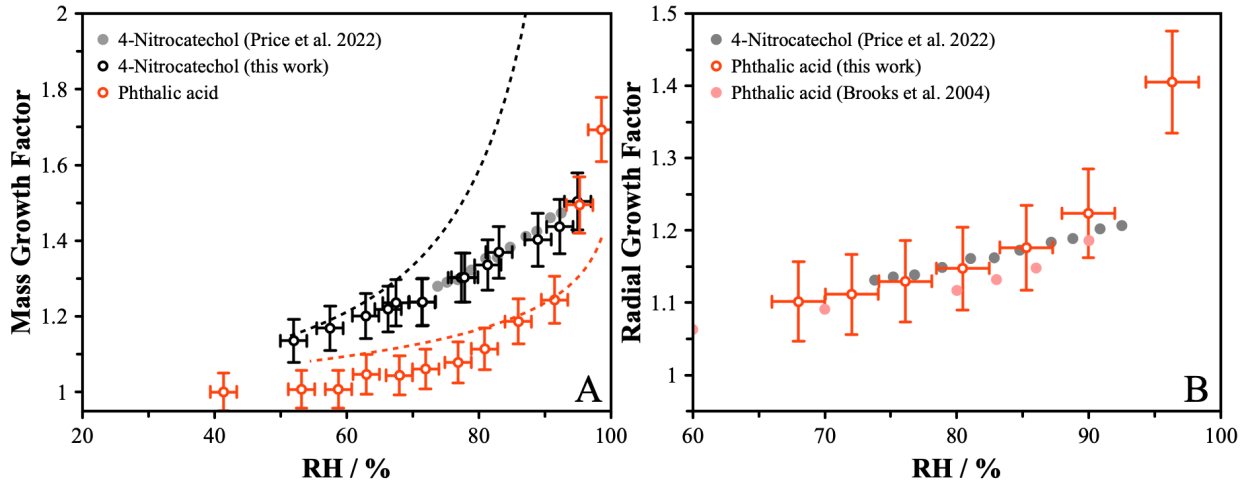

Figure 1: (A) Hygroscopic growth of 4-nitrocatechol derived from this work (black points) and calculated from the radial growth factor data of Price et al. (gray points), and phthalic acid (red points). Data from this work was derived

from three repeat experiments on each sample. The x-error bars are a ±2% uncertainty in the probe RH, and the y-error bars are estimated based on the resolution of the applied voltages and the standard deviation of repeat measurements, leading to a total uncertainty of around ±10%. AIOMFAC predictions are shown by the dash lines. (B) Radial growth factors of 4-nitrocatechol from Price at al.,[35] and phthalic acid from this work and Brooks et al.[50]

The mass and radial growth factors for both phthalic acid and 4-nitrocatechol are shown in Figure 1A and 1B. Both exhibit partial solubility in water and measurable growth due to uptake of water at high RH. The solubility was measured to be 12.2 g/L for 4-nitrocatechol and 6.0 g/L for phthalic acid, indicating that both compounds are highly supersaturated in particles at high RH. Literature data for phthalic acid radial growth factors, determined using a hygroscopic tandem differential mobility analyzer, agree with our data within the uncertainty range.[50] To determine the radial growth factor, we used the DC voltage to estimate the dry size in the presence of a gas flow, subtracting the mass contributions to yield DC voltages directly proportional to the radii, as detailed in our earlier work, due to the linear dependence of Stokes drag forces on size.[51] This procedure allows a dry size to be estimated, but does result in a large uncertainty.

Following efflorescence to form solid particles, at ~50% RH for 4NC and ~55% for PA, neither particle types exhibited deliquescence at experimentally accessible RH conditions, consistent with the water activity measured in the saturated solutions approaching one, discussed in the Supplementary Information. The mass growth data is compared to the output from the Aerosol Inorganic-Organic Mixtures Functional groups Activity Coefficients model (AIOMFAC),[52,53] a popular group contribution model for estimating the thermodynamic properties of compounds in mixtures. The model takes the composition as input and determines the interaction parameters between all species based on the possible short-, mid- and long-range interactions. The output is the activity of each component as a function of composition, which is readily converted to a mass growth factor versus water activity (or RH). The AIOMFAC model overpredicts the hygroscopic growth of 4NC relative to the experiment observations. This is consistent with our earlier work comparing the measured radial growth factors to AIOMFAC predictions via a density approximation.[35] The present work does not require density information and confirms that the deviations cannot be explained by the uncertainty in estimated density. . For PA, the agreement is much closer, with the model predicting slightly higher growth at low RH and less growth at high RH. In 4NC, the model consistently overestimates the growth. These comparisons yield some insights into the intramolecular interactions that might be regulating the thermodynamics, as these are not captured by the AIOMFAC model. For example, in our previous work we showed that the measured hygroscopic growth is closely predicted from a model that assumes ideality if the 4NC molecules existed as dimers in solution.[35] In phthalic acid, the deviations at low RH may be due to the intramolecular bonding possible between the adjacent carboxyl groups, which reduces the extent of intermolecular H-bonding with water.[49] At high RH, we measure a much stronger

affinity of water for the particle phase, which could occur due to partial ionization of one of the acid groups to form a carboxylate, leading to stronger interactions with water and a larger hygroscopicity.

Over the course of 2-3 hours under a lab temperature of 293 K, neither 4NC nor PA particles were observed to change in size due to evaporation, indicating vapor pressures that are $<10^{-5}$ Pa. Compared to the literature data estimates shown in Table 1, the liquid-state[a] vapor pressures of 4NC and PA are determined here to be lower than those reported previously by at least one order of magnitude.[43] The difference in temperature may account for some of the difference, while uncertainties in the methods of estimating liquid-state vapor pressure from solid-state vapor pressures may account for the remaining difference. Based on these observations, it is reasonable to assume that these compounds will remain particle-bound throughout their atmospheric lifetime, even in aqueous solution. Indeed, this is consistent with observations of wildfire smoke particles that show 4NC is primarily particle bound even when aerosol mass concentrations are low following plume dilution.[54] This also indicates favorable gas-to-particle partitioning of compounds with similar volatility in the BB plume.

Aromatic and Nitroaromatic Carbonyls

Unlike 4NC and PA, most of the substituted aromatic and nitroaromatic compounds we measured did not show measurable water uptake at any RH. Particles were generated from aqueous solutions and levitated at high RH (~90 to 95%). Even under these conditions, efflorescence was observed immediately and no subsequent change in the mass of the particles was observed as a function of RH. Figure 2A shows representative hygroscopicity plots for vanillic, syringic and p-hydroxybenzoic acid as examples, with the data all clustered around a mass growth factor of 1, within the uncertainty, across all RH conditions. The same behavior was observed for 2-nitrobenzaldehyde and nitrobenzoic acid. Among these compounds showing no hygroscopic growth were those with O/C ratios higher than PA (nitrobenzoic acid and syringic acid). These compounds are much less soluble in water, as shown in Table 1, and the thermodynamic driving force for solidification in a particle is sufficient to prevent a metastable aqueous phase existing, even at high RH. The hygroscopicity of vanillic, syringic, and p–hydroxybenzoic acid, previously measured using tandem differential mobility analyzer, did not show any significant radial growth at 100 nm particle radius under the RH conditions up to 95%, supporting the observations made here.[55,56] For these three

[a] It should be noted that while the literature often refers to the vapor pressure of the subcooled liquid, these are in fact supercooled liquids, a metastable liquid form of the compound below the melting point. Subcooling is more typically used to refer to a vapor phase that exists below its boiling point. For clarity, in this work we use the terminology liquid-state and solid-state vapor pressures.

compounds, previous work has observed a slight decrease of particle radius at elevated RH. However, in these measurements, as with 4NC and PA, these compounds were not observed to show any measurable change in mass over a 2-3 hour duration, indicating vapor pressures $<10^{-5}$ Pa and consistent with their expected low vapor pressures (see Table 1).

Nitrophenols

Unlike the other compounds explored so far, the three isomers of nitrophenol studied all exhibited measurable volatility and a distinct hygroscopic response. Measurements of the hygroscopic growth of the nitrophenols were complicated by the high rates of evaporation, and only limited data could be obtained for 4-nitrophenol. Instead of probing a single particle across a range of RH conditions, we probed fresh particles at each RH, and then rapidly dried them to estimate the dry mass. This yields the estimated mass growth factors shown in Figure 2B, with a large negative uncertainty arising due to the evaporation that occurs between high RH and low RH measurements. Despite the large uncertainty, we see generally good agreement to the AIOMFAC model. The model does not discriminate between isomers of nitrophenol, which clearly show different thermodynamic properties as evidenced by the different rates of evaporation as a function of RH. We can further assess the hygroscopicity by exploring the rates of evaporation, shown in Figure 3.

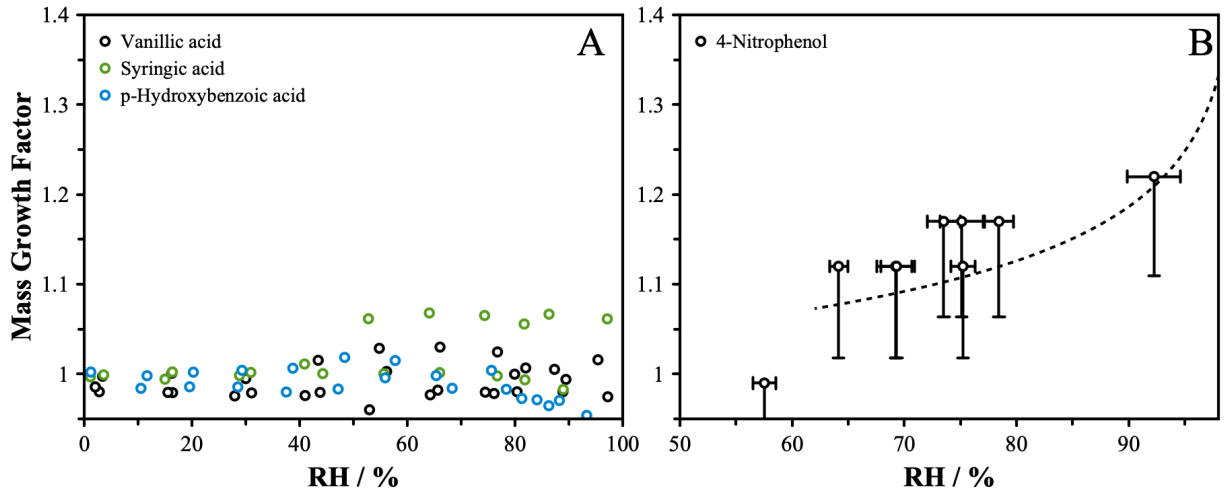

Figure 2: (A) The substituted aromatics vanillic, syringic and para-hydroxybenzoic acid show no hygroscopic response up to ~96% RH. (B) The hygroscopic growth of 4-nitrophenol was determined through measurements on individual particles at each RH in order to minimize the extent of evaporation; the lower error bound encompasses the systematic errors associated with particle evaporation during the measurement. Efflorescence was observed at around 60% RH. The black dash line indicates the AIOMFAC prediction.

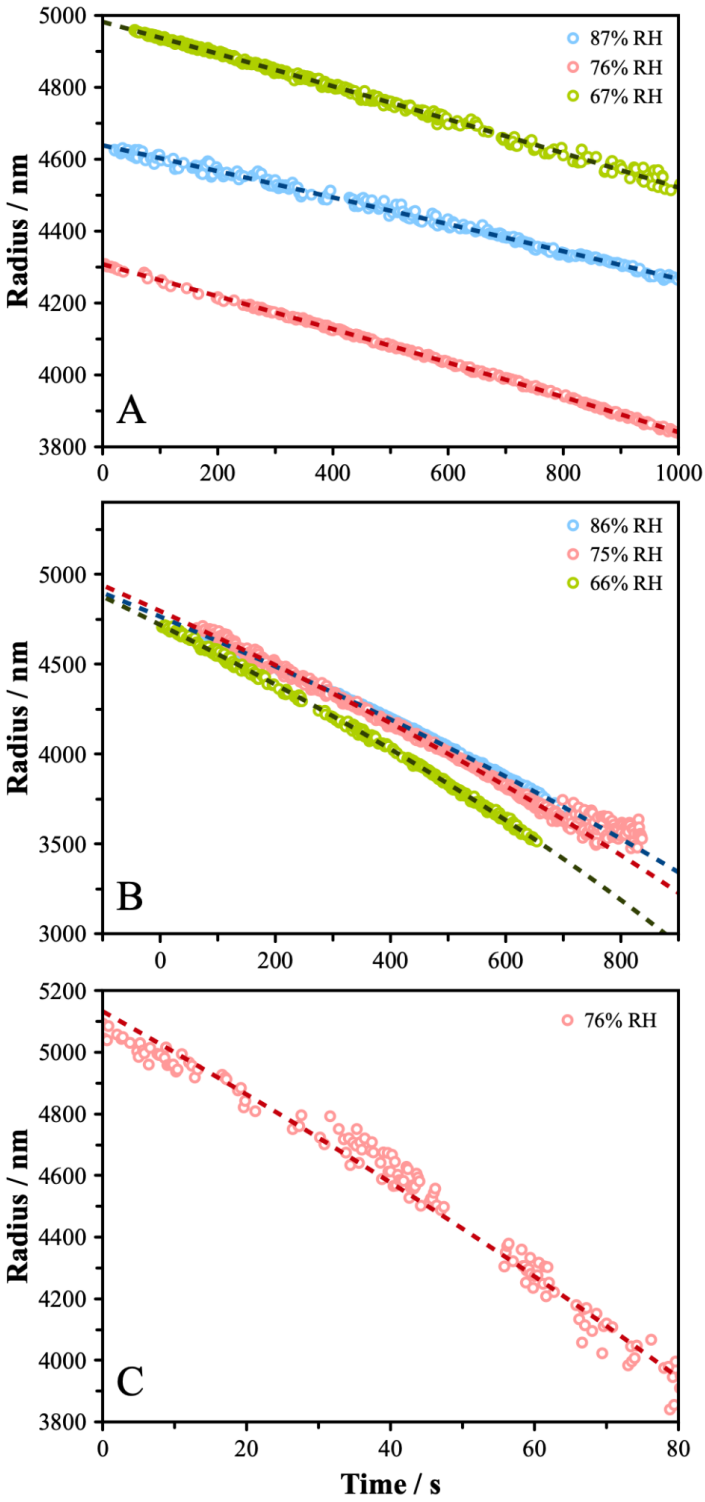

Figure 3: Evaporation measurements were performed for (A) 4-nitrophenol; (B) 3-nitrophenol and (C) 2-nitrophenol under a range of RH conditions that yielded aqueous spherical particles. The uncertainty in the size is ±5 nm based on the accuracy of the Mie resonance sizing algorithm. A linear fit to the radius-squared vs time is shown for each dataset by the dash line. The evaporation rates and calculated vapor pressures are reported in Table 2.

The evaporation of NP particles was measured for each isomer across a range of RH conditions, where possible. The evaporation model, presented in Equation 4, predicts a linear dependence of the radius-squared versus time, consistent with the measured evaporation of the nitrophenol compounds shown in Figure 3. From the slope of radius-squared versus time we obtain the evaporation rates shown in Table 2. The AIOMFAC model was used to obtain the mass ratio of water, which is assumed to be the same for all isomers.[52,53] Solving for the pure component vapor pressure yields 0.010 ± 0.03, 0.036 ± 0.011, and 0.35 ± 0.11 Pa for 4-nitrophenol, 3-nitrophenol and 2-nitrophenol, respectively at 293K, revealing more than one order of magnitude variation in the volatility across the isomers. Importantly, accounting for the amount of water effectively eliminates the dependence on RH, indicating the hygroscopicity is well described by the AIOMFAC model. The uncertainty in the reported vapor pressures arise from the gas phase diffusion coefficient and the uncertainty in the mole fraction of water.

These values we report here show some differences from the literature estimates of the vapor pressure of the liquid state that are based on subcooled correction using the Prausnitz equation,[48] which rely on accurate solid-state data and other thermochemical properties. The experimental vapor pressure of 3-nitrophenol in our study (0.036 Pa at 293 K) is slightly above the literature value of 0.0114[48] Pa at 298 K obtained using Knudsen effusion mass spectrometry (KEMS) and differential scanning calorimetry (DSC). Previous studies have found out that the vapor pressure of nitrophenols obtained from solid-state data is sensitive to the reference compound used in the study.[49] For instance, subcooled vapor pressure of 4NP derived from KEMS and DSC was 5.14 x 10^{-3} Pa at 298 K, with an estimated error of $\pm 75\%$,[48] whilst data derived from gas chromatography retention data using 2-nitrophenol as the reference was 0.11 Pa at 293 K, which was reported to be a largely overestimated value.[47] Vapor pressure measurements made using similar techniques have agreed with each other,[43] although direct measurements of evaporation from liquid-state samples, as in our work, have not previously been reported. We demonstrate that the vapor pressures are actually much higher than expected based on previous literature, indicating that the amount of particle bound nitrophenol may be less than predicted. However, other factors may influence volatility, such as deprotonation that may lead to reduced volatility and increased solubility, stabilizing the nitrophenols in the aqueous phase.[57] The pKa values of 4-nitrophenol, 3-nitrophenol, and 2-nitrophenol are about 7.2, 8.4, and 7.2 respectively.[58] This indicates that in basic atmospheric aerosol or droplets, nitrophenols are mostly present in the deprotonated form, and in acidic environments, these are mostly present in the protonated form. Thus, pH of the aerosol particle may affect the hygroscopicity, volatility, and optical properties of nitrophenols.[59]

Table 2: Thermodynamic data (mole fraction (x_{org}) and activity coefficient (γ_{org}) of the organic) derived from the AIOMFAC model, measured evaporation rates ($\frac{da^2}{dt}$), and calculated vapor pressures according to Equations 3 and 4

for p_{eff} and p_{org} respectively. The data shown in italics represents measurements under dry conditions using either radial data or mass spectrometry data, as described in the text.

	RH / %	x_{org}	γ_{org}	da^2/dt / m^2 s^{-1}	p_{eff} / Pa	p_{org} / Pa
4NP	87	0.44	1.11	3.31×10^{15}	5.44×10^{-3}	9.6×10^{-3}
4NP	76	0.54	1.05	3.81×10^{-15}	6.26×10^{-3}	9.9×10^{-3}
4NP	67	0.61	1.03	4.38×10^{15}	7.20×10^{-3}	1.1×10^{-2}
4NP (MS)	*0*	*1*	*1*	*2.86×10^{15}*	*N/A*	*4.7×10^{-3}*
3NP	86	0.45	1.11	1.28×10^{14}	2.11×10^{-2}	3.6×10^{-2}
3NP	75	0.55	1.05	1.40×10^{14}	2.30×10^{-2}	3.6×10^{-2}
3NP	66	0.61	1.03	1.51×10^{14}	2.49×10^{-2}	3.7×10^{-2}
3NP (radial)	*0*	*1*	*1*	*2.85×10^{14}*	*N/A*	*4.7×10^{-2}*
3NP (MS)	*0*	*1*	*1*	*3.2×10^{14}*	*N/A*	*5.2×10^{-2}*
2NP	76	0.54	1.05	1.35×10^{13}	0.22	0.35

The variation in p_{org} can be interpreted in terms of the molecular interactions between organic molecules. In 4-nitrophenol (para), the OH group and the NO_2 group are not directly interacting due to the separation, with intramolecular H-bonding not possible. Instead, H-bonding with water and other 4-nitrophenol molecules will dominate, stabilizing the molecule in solution. As the functional groups get closer, the intramolecular bonding becomes more significant, and the 3- (meta) and 2- (ortho) isomers become less stabilized in solution leading to a greater vapor pressure. This is opposite to the trend seen in the solid-state for some substituted nitroaromatic compounds,[43] however a general trend between ortho-, meta- and para-positions of functional groups has not been identified. In field campaigns that have measured nitrophenol content, the concentration of 4-nitrophenol is often higher than 2-nitrophenol in both condensed phase and gas phase,[60,61] and 4-nitrophenol has also been detected in cloud water samples.[17] Our data suggest that rate of evaporation of 4-nitrophenol is up to a hundred times slower than that of 2-nitrophenol, and bulk solubility of 4-nitrophenol is approximately five times higher than that of 2-nitrophenol, which enhances the partitioning of 4-nitrophenol into the condensed phase. Other factors may contribute to variations in the abundance of different isomers, such as their formation yields and subsequent reactivity.

To investigate the influence of particle phase state on the rate of evaporation, additional measurements were performed under dry conditions, leading to non-spherical solid-state particles forming for 4-nitrophenol and 2-nitrophenol. Mie resonance sizing is not possible for non-spherical particles, and we used our established open-port sampling interface mass spectrometry (OPSI-MS) method to probe the rate of evaporation, as described in the Supplementary Information and our earlier work.[62] These data are shown in Figure 4A for 4-nitrophenol. The rate of evaporation is much slower than observed at high RH, for aqueous particles, and a vapor pressure of 4.7×10^{-3} Pa was calculated, which is just under half the value determined for the liquid state. In the case of 3-nitrophenol, the evaporation rate was slightly faster than the aqueous particles, yielding a vapor pressure of 5.2×10^{-3} Pa (Figure 4B). Interestingly, dry 3-nitrophenol particles continued to exhibit a spherical geometry, indicating they remained amorphous and did not solidify under the experimental conditions. The radius evolution yields an estimated vapor pressure in close agreement to the OPSI-MS data (Figure 4C). The calculations and relevant data are tabulated in Table 2. Measurements of solid 2-nitrophenol particles were not possible due to low signal in the MS and the rapid evaporation rate, even under dry conditions.

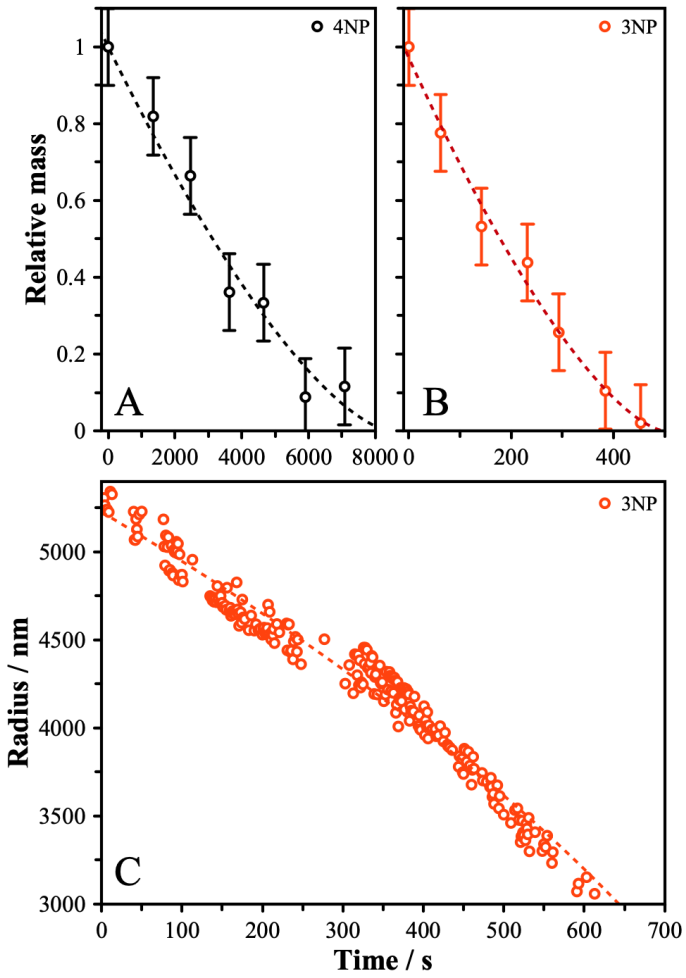

Figure 4: (A) The relative mass change for solid-state particles of 4NP obtained using the LQ-EDB coupled with OPSI-MS. (B) The relative mass change for particles of 3-NP under dry conditions, which exhibited an amorphous morphology. Errors bars in both panels show the expected variability in the measured relative mass for a single particle. The dashed lines represent fits to the function $m = (R't + 1)^{\frac{3}{2}}$, where m is the relative mass and R' is a normalized evaporation rate, which may be converted to a radius-squared evaporation rate by assuming a known starting radius. (C) Amorphous particles of 3NP remained spherical and exhibited rapid evaporation before solidification occurred and the evaporation process stopped. The red dash line represents a fit to the function $a = (Rt + a_0)^{0.5}$, where a is the radius, t is time, and a_0 is the starting radius, and indicates a constant radius-squared evaporation rate (R).

Conclusions

The hygroscopicity and volatility of biomass burning compounds will influence their fate in the atmosphere. Using a newly developed method to measure mass hygroscopic growth factors in a linear quadrupole EDB, validated using NaCl and $(NH_4)_2SO_4$, the hygroscopicity of pure substituted aromatic constituents that are found in biomass burning aerosols were measured. 4-Nitrocatechol and phthalic acid were the most hygroscopic compounds, showing measurable and reversible water uptake under subsaturated RH conditions until the point of efflorescence. Mass growth data were compared with AIOMFAC model

predictions, supporting earlier assertions that intramolecular interactions reduce the hygroscopicity relative to the functional group contribution model, showing the importance of considering intramolecular interactions when predicting the hygroscopicity of aromatic OA constituents. Unlike phthalic acid, other substituted benzoic acid particles do not show measurable water uptake, in spite of similar or higher O/C ratios than phthalic acid, likely due to their low bulk water solubility and different molecular interactions between functional groups. Therefore, predicting the hygroscopicity of OA compounds is complex and should consider bulk water solubility, O/C ratio, molecular weight, and most importantly intramolecular interactions arising from the molecular structure. Understanding the strength of intramolecular interactions versus intermolecular hydrogen bonds between water and solute molecules would add more insight to predict the hygroscopicity of OA, which may be facilitated by future studies on using computational methods. In our measurements following efflorescence to produce a solid particle, none of the organic compounds studied exhibit deliquescence at experimentally accessible RH conditions (~95%), consistent with bulk water activity measured for the saturated solutions approaching unity. This indicates that in the atmosphere, it will only be after cloud forming conditions have been approached that aerosol particles containing these compounds will remain as aqueous particles. The role of organic and inorganic co-solutes is not considered here, but represents a clear direction for future measurements to assess the influence of BB aerosol of greater chemical complexity. Overall, our measurements indicates that the hygroscopicity of BB aerosol particles may be driven by relatively few organic species and highly hygroscopicity particles particles may be largely influenced by salts that are entrained in the particles.

A major factor that determines the lifetime of particles in the atmosphere is the volatility of its individual components. Field studies have identified that BrC compound concentrations emitted from wildfire plumes, such as 4-nitrocatechol, are lost over the atmospheric transport with an approximate half life of 9h -15h.[63] Based on its low volatility, we suggest 4-nitrocatechol is mostly lost due to particle phase reactions rather than their evaporation to the gas phase, possibly via photolysis.[64] The same conclusions may be applied to all compounds studied here, except for the nitrophenol isomers. All isomers of nitrophenol exhibited measurable volatility under the experimental timescales and temperature. Particle evaporation measurements allow us to calculate the vapor pressure of these compounds, revealing more than one order of magnitude variation in the volatility across the isomers. We demonstrate that the experimental vapor pressure of the nitrophenol isomers is much higher than literature data, which rely on model-based corrections to measured solid-state vapor pressure. Under dry conditions, particles of 3NP exhibited an amorphous state that exhibited a vapor pressure consistent with the estimated vapor pressure from the aqueous state. However, both 2NP and 4NP solidified, and mass spectrometry measurements of the evaporation rates of these solid particles reveal a decrease in vapor pressure of 4NP to around half the

liquid-state value. The measured presence of NP in ambient aerosol particles indicates that some mechanism exists to retain NP in the particle phase. The additional chemical complexity of ambient particles may allow the compounds to bind more strongly to the condensed phase through additional molecular interactions, such as with ionic species, or remain bound to the particle phase due to slow diffusion induced by high viscosity at low RH and low temperature. These effects are as yet unresolved but point towards future research to fully classify the behavior of BB aerosol.

Overall, the measurements reported here provide some additional clarity on the microphysical properties of particles containing a range of BB compounds, while also identifying important avenues for future research. Given the chemical complexity of real biomass burning emissions, being able to predict the behavior based on the contributions from individual components, and to identify when additional information is required, is a vital step in characterizing the impacts and lifetime of real aerosol particles.

Acknowledgements

All authors acknowledge the support of the National Science Foundation through grant AGS-2144005.

Supporting Information

Additional method descriptions and validation measurements.

References

(1) Ramnarine, E.; Kodros, J. K.; Hodshire, A. L.; Lonsdale, C. R.; Alvarado, M. J.; Pierce, J. R. Effects of Near-Source Coagulation of Biomass Burning Aerosols on Global Predictions of Aerosol Size Distributions and Implications for Aerosol Radiative Effects. *Atmospheric Chemistry and Physics* **2019**, *19* (9), 6561–6577. https://doi.org/10.5194/acp-19-6561-2019.

(2) Suzuki, K.; Takemura, T. Perturbations to Global Energy Budget Due to Absorbing and Scattering Aerosols. *J. Geophys. Res. Atmos.* **2019**, *124* (4), 2194–2209. https://doi.org/10.1029/2018JD029808.

(3) Li, J.; Carlson, B. E.; Yung, Y. L.; Lv, D.; Hansen, J.; Penner, J. E.; Liao, H.; Ramaswamy, V.; Kahn, R. A.; Zhang, P.; Dubovik, O.; Ding, A.; Lacis, A. A.; Zhang, L.; Dong, Y. Scattering and Absorbing Aerosols in the Climate System. *Nat Rev Earth Environ* **2022**, *3* (6), 363–379. https://doi.org/10.1038/s43017-022-00296-7.

(4) Mahowald, N. Aerosol Indirect Effect on Biogeochemical Cycles and Climate. *Science* **2011**. https://doi.org/10.1126/science.1207374.

(5) Akagi, S. K.; Yokelson, R. J.; Wiedinmyer, C.; Alvarado, M. J.; Reid, J. S.; Karl, T.; Crounse, J. D.; Wennberg, P. O. Emission Factors for Open and Domestic Biomass Burning for Use in Atmospheric Models. *Atmos. Chem. Phys.* **2011**, *11* (9), 4039–4072. https://doi.org/10.5194/acp-11-4039-2011.

(6) Shaik, D. S.; Kant, Y.; Sateesh, M.; Sharma, V.; Rawat, D. S.; Chandola, H. C. Spatio-Temporal Variation of Biomass Burning Fires over Indian Region Using Satellite Data. In *Atmospheric Remote Sensing*; Elsevier, 2023; pp 121–138. https://doi.org/10.1016/B978-0-323-99262-6.00009-2.

(7) Reisen, F.; Meyer, C. P. (Mick); Keywood, M. D. Impact of Biomass Burning Sources on Seasonal Aerosol Air Quality. *Atmospheric Environment* **2013**, *67*, 437–447. https://doi.org/10.1016/j.atmosenv.2012.11.004.

(8) Ballesteros-González, K.; Sullivan, A. P.; Morales-Betancourt, R. Estimating the Air Quality and Health Impacts of Biomass Burning in Northern South America Using a Chemical Transport Model. *Science of The Total Environment* **2020**, *739*, 139755. https://doi.org/10.1016/j.scitotenv.2020.139755.

(9) Thornhill, G. D.; Ryder, C. L.; Highwood, E. J.; Shaffrey, L. C.; Johnson, B. T. The Effect of South American Biomass Burning Aerosol Emissions on the Regional Climate. *Atmospheric Chemistry and Physics* **2018**, *18* (8), 5321–5342. https://doi.org/10.5194/acp-18-5321-2018.

(10) Andreae, M. O. Emission of Trace Gases and Aerosols from Biomass Burning – an Updated Assessment. *Atmos. Chem. Phys.* **2019**, *19* (13), 8523–8546. https://doi.org/10.5194/acp-19-8523-2019.

(11) Lin, P.; Fleming, L. T.; Nizkorodov, S. A.; Laskin, J.; Laskin, A. Comprehensive Molecular Characterization of Atmospheric Brown Carbon by High Resolution Mass Spectrometry with Electrospray and Atmospheric Pressure Photoionization. *Anal. Chem.* **2018**, *90* (21), 12493–12502. https://doi.org/10.1021/acs.analchem.8b02177.

(12) Guo, H.; Wang, Y.; Yao, K.; Zheng, H.; Zhang, X.; Li, R.; Wang, N.; Fu, H. The Overlooked Formation of Environmentally Persistent Free Radicals on Particulate Matter Collected from Biomass Burning under Light Irradiation. *Environment International* **2023**, *171*, 107668. https://doi.org/10.1016/j.envint.2022.107668.

(13) Lin, P.; Aiona, P. K.; Li, Y.; Shiraiwa, M.; Laskin, J.; Nizkorodov, S. A.; Laskin, A. Molecular Characterization of Brown Carbon in Biomass Burning Aerosol Particles. *Environ. Sci. Technol.* **2016**, *50* (21), 11815–11824. https://doi.org/10.1021/acs.est.6b03024.

(14) Laskin, A.; Laskin, J.; Nizkorodov, S. A. Chemistry of Atmospheric Brown Carbon. *Chem. Rev.* **2015**, *115* (10), 4335–4382. https://doi.org/10.1021/cr5006167.

(15) Andreae, M. O.; Gelencsér, A. Black Carbon or Brown Carbon? The Nature of Light-Absorbing Carbonaceous Aerosols. *Atmospheric Chemistry and Physics* **2006**, *6* (10), 3131–3148. https://doi.org/10.5194/acp-6-3131-2006.

(16) Updyke, K. M.; Nguyen, T. B.; Nizkorodov, S. A. Formation of Brown Carbon via Reactions of Ammonia with Secondary Organic Aerosols from Biogenic and Anthropogenic Precursors. *Atmospheric Environment* **2012**, *63*, 22–31. https://doi.org/10.1016/j.atmosenv.2012.09.012.

(17) Desyaterik, Y.; Sun, Y.; Shen, X.; Lee, T.; Wang, X.; Wang, T.; Collett, J. L. Speciation of "Brown" Carbon in Cloud Water Impacted by Agricultural Biomass Burning in Eastern China: "BROWN" CARBON SPECIATION IN CLOUD WATER. *J. Geophys. Res. Atmos.* **2013**, *118* (13), 7389–7399. https://doi.org/10.1002/jgrd.50561.

(18) Mohr, C.; Lopez-Hilfiker, F. D.; Zotter, P.; Prévôt, A. S. H.; Xu, L.; Ng, N. L.; Herndon, S. C.; Williams, L. R.; Franklin, J. P.; Zahniser, M. S.; Worsnop, D. R.; Knighton, W. B.; Aiken, A. C.; Gorkowski, K. J.; Dubey, M. K.; Allan, J. D.; Thornton, J. A. Contribution of Nitrated Phenols to Wood Burning Brown Carbon Light Absorption in Detling, United Kingdom during Winter Time. *Environ. Sci. Technol.* **2013**, *47* (12), 6316–6324. https://doi.org/10.1021/es400683v.

(19) Li, X.; Jiang, L.; Hoa, L. P.; Lyu, Y.; Xu, T.; Yang, X.; Iinuma, Y.; Chen, J.; Herrmann, H. Size Distribution of Particle-Phase Sugar and Nitrophenol Tracers during Severe Urban Haze Episodes in Shanghai. *Atmospheric Environment* **2016**, *145*, 115–127. https://doi.org/10.1016/j.atmosenv.2016.09.030.
(20) El-Sayed, M. M. H.; Hennigan, C. J. Aqueous Processing of Water-Soluble Organic Compounds in the Eastern United States during Winter. *Environ. Sci.: Processes Impacts* **2023**, *25* (2), 241–253. https://doi.org/10.1039/D2EM00115B.
(21) Simoneit, B. R. T. Biomass Burning — a Review of Organic Tracers for Smoke from Incomplete Combustion. *Applied Geochemistry* **2002**, *17* (3), 129–162. https://doi.org/10.1016/S0883-2927(01)00061-0.
(22) Burgay, F.; Salionov, D.; Huber, C. J.; Singer, T.; Eichler, A.; Ungeheuer, F.; Vogel, A.; Schwikowski, M.; Bjelić, S. Hybrid Targeted/Untargeted Screening Method for the Determination of Wildfire and Water-Soluble Organic Tracers in Ice Cores and Snow. *Anal. Chem.* **2023**, *95* (30), 11456–11466. https://doi.org/10.1021/acs.analchem.3c01852.
(23) Hatch, L. E.; Rivas-Ubach, A.; Jen, C. N.; Lipton, M.; Goldstein, A. H.; Barsanti, K. C. Measurements of I/SVOCs in Biomass-Burning Smoke Using Solid-Phase Extraction Disks and Two-Dimensional Gas Chromatography. *Atmos. Chem. Phys.* **2018**, *18* (24), 17801–17817. https://doi.org/10.5194/acp-18-17801-2018.
(24) Akherati, A.; He, Y.; Coggon, M. M.; Koss, A. R.; Hodshire, A. L.; Sekimoto, K.; Warneke, C.; De Gouw, J.; Yee, L.; Seinfeld, J. H.; Onasch, T. B.; Herndon, S. C.; Knighton, W. B.; Cappa, C. D.; Kleeman, M. J.; Lim, C. Y.; Kroll, J. H.; Pierce, J. R.; Jathar, S. H. Oxygenated Aromatic Compounds Are Important Precursors of Secondary Organic Aerosol in Biomass-Burning Emissions. *Environ. Sci. Technol.* **2020**, *54* (14), 8568–8579. https://doi.org/10.1021/acs.est.0c01345.
(25) Hennigan, C. J.; Miracolo, M. A.; Engelhart, G. J.; May, A. A.; Presto, A. A.; Lee, T.; Sullivan, A. P.; McMeeking, G. R.; Coe, H.; Wold, C. E.; Hao, W.-M.; Gilman, J. B.; Kuster, W. C.; De Gouw, J.; Schichtel, B. A.; Collett, J. L.; Kreidenweis, S. M.; Robinson, A. L. Chemical and Physical Transformations of Organic Aerosol from the Photo-Oxidation of Open Biomass Burning Emissions in an Environmental Chamber. *Atmos. Chem. Phys.* **2011**, *11* (15), 7669–7686. https://doi.org/10.5194/acp-11-7669-2011.
(26) Palm, B. B.; Peng, Q.; Fredrickson, C. D.; Lee, B. H.; Garofalo, L. A.; Pothier, M. A.; Kreidenweis, S. M.; Farmer, D. K.; Pokhrel, R. P.; Shen, Y.; Murphy, S. M.; Permar, W.; Hu, L.; Campos, T. L.; Hall, S. R.; Ullmann, K.; Zhang, X.; Flocke, F.; Fischer, E. V.; Thornton, J. A. Quantification of Organic Aerosol and Brown Carbon Evolution in Fresh Wildfire Plumes. *Proc. Natl. Acad. Sci. U.S.A.* **2020**, *117* (47), 29469–29477. https://doi.org/10.1073/pnas.2012218117.
(27) May, A. A.; Lee, T.; McMeeking, G. R.; Akagi, S.; Sullivan, A. P.; Urbanski, S.; Yokelson, R. J.; Kreidenweis, S. M. Observations and Analysis of Organic Aerosol Evolution in Some Prescribed Fire Smoke Plumes. *Atmos. Chem. Phys.* **2015**, *15* (11), 6323–6335. https://doi.org/10.5194/acp-15-6323-2015.
(28) Kroll, J. H.; Seinfeld, J. H. Chemistry of Secondary Organic Aerosol: Formation and Evolution of Low-Volatility Organics in the Atmosphere. *Atmospheric Environment* **2008**, *42* (16), 3593–3624. https://doi.org/10.1016/j.atmosenv.2008.01.003.
(29) Graham, E. L.; Wu, C.; Bell, D. M.; Bertrand, A.; Haslett, S. L.; Baltensperger, U.; El Haddad, I.; Krejci, R.; Riipinen, I.; Mohr, C. Volatility of Aerosol Particles from NO_3 Oxidation of Various Biogenic Organic Precursors. *Atmospheric Chemistry and Physics* **2023**, *23* (13), 7347–7362. https://doi.org/10.5194/acp-23-7347-2023.
(30) Kalberer, M.; Sax, M.; Samburova, V. Molecular Size Evolution of Oligomers in Organic Aerosols Collected in Urban Atmospheres and Generated in a Smog Chamber. *Environ. Sci. Technol.* **2006**, *40* (19), 5917–5922. https://doi.org/10.1021/es0525760.
(31) Häkkinen, S. A. K.; McNeill, V. F.; Riipinen, I. Effect of Inorganic Salts on the Volatility of Organic Acids. *Environ. Sci. Technol.* **2014**, *48* (23), 13718–13726. https://doi.org/10.1021/es5033103.
(32) Hu, W.; Palm, B. B.; Day, D. A.; Campuzano-Jost, P.; Krechmer, J. E.; Peng, Z.; de Sá, S. S.; Martin, S. T.; Alexander, M. L.; Baumann, K.; Hacker, L.; Kiendler-Scharr, A.; Koss, A. R.; de Gouw, J. A.; Goldstein, A. H.; Seco, R.; Sjostedt, S. J.; Park, J.-H.; Guenther, A. B.; Kim, S.; Canonaco, F.; Prévôt, A. S. H.; Brune, W. H.; Jimenez, J. L. Volatility and Lifetime against OH Heterogeneous Reaction of Ambient Isoprene-Epoxydiols-Derived Secondary Organic Aerosol (IEPOX-SOA). *Atmospheric Chemistry and Physics* **2016**, *16* (18), 11563–11580. https://doi.org/10.5194/acp-16-11563-2016.
(33) McNeill, V. F.; Yatavelli, R. L. N.; Thornton, J. A.; Stipe, C. B.; Landgrebe, O. Heterogeneous OH Oxidation of Palmitic Acid in Single Component and Internally Mixed Aerosol Particles: Vaporization and the Role of Particle Phase. *Atmospheric Chemistry and Physics* **2008**, *8* (17), 5465–5476. https://doi.org/10.5194/acp-8-5465-2008.

(34) Marsh, A.; Miles, R. E. H.; Rovelli, G.; Cowling, A. G.; Nandy, L.; Dutcher, C. S.; Reid, J. P. Influence of Organic Compound Functionality on Aerosol Hygroscopicity: Dicarboxylic Acids, Alkyl-Substituents, Sugars and Amino Acids. *Atmos. Chem. Phys.* **2017**, *17* (9), 5583–5599. https://doi.org/10.5194/acp-17-5583-2017.
(35) Price, C. L.; Preston, T. C.; Davies, J. F. Hygroscopic Growth, Phase Morphology, and Optical Properties of Model Aqueous Brown Carbon Aerosol. *Environ. Sci. Technol.* **2022**, *56* (7), 3941–3951. https://doi.org/10.1021/acs.est.1c07356.
(36) Rickards, A. M. J.; Miles, R. E. H.; Davies, J. F.; Marshall, F. H.; Reid, J. P. *Measurements of the Sensitivity of Aerosol Hygroscopicity and the κ Parameter to the O/C Ratio*. ACS Publications. https://doi.org/10.1021/jp407991n.
(37) Han, S.; Hong, J.; Luo, Q.; Xu, H.; Tan, H.; Wang, Q.; Tao, J.; Zhou, Y.; Peng, L.; He, Y.; Shi, J.; Ma, N.; Cheng, Y.; Su, H. Hygroscopicity of Organic Compounds as a Function of Organic Functionality, Water Solubility, Molecular Weight, and Oxidation Level. *Atmospheric Chemistry and Physics* **2022**, *22* (6), 3985–4004. https://doi.org/10.5194/acp-22-3985-2022.
(38) Chan, M. N.; Choi, M. Y.; Ng, N. L.; Chan, C. K. Hygroscopicity of Water-Soluble Organic Compounds in Atmospheric Aerosols: Amino Acids and Biomass Burning Derived Organic Species. *Environ. Sci. Technol.* **2005**, *39* (6), 1555–1562. https://doi.org/10.1021/es049584l.
(39) Mouton, M.; Malek, K. A.; James, M. H.; Pokhrel, R. P.; Fiddler, M. N.; Asa-Awuku, A. A.; Bililign, S. The Hygroscopic Properties of Biomass Burning Aerosol from Eucalyptus and Cow Dung under Different Combustion Conditions. *Aerosol Science and Technology* **2023**, *57* (7), 665–677. https://doi.org/10.1080/02786826.2023.2198587.
(40) Betz, K. L.; Calvert, C. T.; Al-Mashala, H. H.; Schnitzler, E. G. Hygroscopicity of Secondary Brown Carbon Aerosol from Aqueous Photo-Oxidation of Phenolic Precursors. *ACS Earth Space Chem.* **2022**, *6* (11), 2609–2618. https://doi.org/10.1021/acsearthspacechem.2c00132.
(41) Price, C. L.; Bain, A.; Wallace, B. J.; Preston, T. C.; Davies, J. F. Simultaneous Retrieval of the Size and Refractive Index of Suspended Droplets in a Linear Quadrupole Electrodynamic Balance. *J. Phys. Chem. A* **2020**, *124* (9), 1811–1820. https://doi.org/10.1021/acs.jpca.9b10748.
(42) Kohli, R. K.; Davies, J. F. Measuring the Chemical Evolution of Levitated Particles: A Study on the Evaporation of Multicomponent Organic Aerosol. *Anal. Chem.* **2021**, *93* (36), 12472–12479. https://doi.org/10.1021/acs.analchem.1c02890.
(43) Booth, A. M.; Bannan, T.; McGillen, M. R.; Barley, M. H.; Topping, D. O.; McFiggans, G.; Percival, C. J. The Role of Ortho, Meta, Para Isomerism in Measured Solid State and Derived Sub-Cooled Liquid Vapour Pressures of Substituted Benzoic Acids. *RSC Adv.* **2012**, *2* (10), 4430–4443. https://doi.org/10.1039/C2RA01004F.
(44) Queimada, A. J.; Mota, F. L.; Pinho, S. P.; Macedo, E. A. *Solubilities of Biologically Active Phenolic Compounds: Measurements and Modeling*. ACS Publications. https://doi.org/10.1021/jp808683y.
(45) Vilas-Boas, S. M.; Vieira, V.; Brandão, P.; Alves, R. S.; Coutinho, J. A. P.; Pinho, S. P.; Ferreira, O. Solvent and Temperature Effects on the Solubility of Syringic, Vanillic or Veratric Acids: Experimental, Modeling and Solid Phase Studies. *Journal of Molecular Liquids* **2019**, *289*, 111089. https://doi.org/10.1016/j.molliq.2019.111089.
(46) Gracin, S.; Rasmuson, Å. C. Solubility of Phenylacetic Acid, *p* -Hydroxyphenylacetic Acid, *p* -Aminophenylacetic Acid, *p* -Hydroxybenzoic Acid, and Ibuprofen in Pure Solvents. *J. Chem. Eng. Data* **2002**, *47* (6), 1379–1383. https://doi.org/10.1021/je0255170.
(47) Schwarzenbach, R. P.; Stierli, Ruth.; Folsom, B. R.; Zeyer, Josef. Compound Properties Relevant for Assessing the Environmental Partitioning of Nitrophenols. *Environ. Sci. Technol.* **1988**, *22* (1), 83–92. https://doi.org/10.1021/es00166a009.
(48) Bannan, T. J.; Booth, A. M.; Jones, B. T.; O'Meara, S.; Barley, M. H.; Riipinen, I.; Percival, C. J.; Topping, D. Measured Saturation Vapor Pressures of Phenolic and Nitro-Aromatic Compounds. *Environ. Sci. Technol.* **2017**, *51* (7), 3922–3928. https://doi.org/10.1021/acs.est.6b06364.
(49) Shelley, P. D.; Bannan, T. J.; Worrall, S. D.; Alfarra, M. R.; Krieger, U. K.; Percival, C. J.; Garforth, A.; Topping, D. Measured Solid State and Subcooled Liquid Vapour Pressures of Nitroaromatics Using Knudsen Effusion Mass Spectrometry. *Atmos. Chem. Phys.* **2020**, *20* (14), 8293–8314. https://doi.org/10.5194/acp-20-8293-2020.
(50) Brooks, S. D.; DeMott, P. J.; Kreidenweis, S. M. Water Uptake by Particles Containing Humic Materials and Mixtures of Humic Materials with Ammonium Sulfate. *Atmospheric Environment* **2004**, *38* (13), 1859–1868. https://doi.org/10.1016/j.atmosenv.2004.01.009.

(51) Davies, J. F.; Price, C. L.; Choczynski, J.; Kohli, R. K. Hygroscopic Growth of Simulated Lung Fluid Aerosol Particles under Ambient Environmental Conditions. *Chem. Commun.* **2021**, *57* (26), 3243–3246. https://doi.org/10.1039/D1CC00066G.
(52) Zuend, A.; Marcolli, C.; Luo, B. P.; Peter, T. A Thermodynamic Model of Mixed Organic-Inorganic Aerosols to Predict Activity Coefficients. *Atmospheric Chemistry and Physics* **2008**, *8* (16), 4559–4593. https://doi.org/10.5194/acp-8-4559-2008.
(53) Zuend, A.; Marcolli, C.; Booth, A. M.; Lienhard, D. M.; Soonsin, V.; Krieger, U. K.; Topping, D. O.; McFiggans, G.; Peter, T.; Seinfeld, J. H. New and Extended Parameterization of the Thermodynamic Model AIOMFAC: Calculation of Activity Coefficients for Organic-Inorganic Mixtures Containing Carboxyl, Hydroxyl, Carbonyl, Ether, Ester, Alkenyl, Alkyl, and Aromatic Functional Groups. *Atmos. Chem. Phys.* **2011**, *11* (17), 9155–9206. https://doi.org/10.5194/acp-11-9155-2011.
(54) Liang, Y.; Wernis, R. A.; Kristensen, K.; Kreisberg, N. M.; Croteau, P. L.; Herndon, S. C.; Chan, A. W. H.; Ng, N. L.; Goldstein, A. H. Gas–Particle Partitioning of Semivolatile Organic Compounds When Wildfire Smoke Comes to Town. *Atmospheric Chemistry and Physics* **2023**, *23* (19), 12441–12454. https://doi.org/10.5194/acp-23-12441-2023.
(55) Mochida, M.; Kawamura, K. Hygroscopic Properties of Levoglucosan and Related Organic Compounds Characteristic to Biomass Burning Aerosol Particles: HYGROSCOPIC PROPERTY OF LEVOGLUCOSAN. *J. Geophys. Res.* **2004**, *109* (D21), n/a-n/a. https://doi.org/10.1029/2004JD004962.
(56) Lei, T.; Zuend, A.; Wang, W. G.; Zhang, Y. H.; Ge, M. F. Hygroscopicity of Organic Compounds from Biomass Burning and Their Influence on the Water Uptake of Mixed Organic Ammonium Sulfate Aerosols. *Atmos. Chem. Phys.* **2014**, *14* (20), 11165–11183. https://doi.org/10.5194/acp-14-11165-2014.
(57) Wang, H.; Gao, Y.; Wang, S.; Wu, X.; Liu, Y.; Li, X.; Huang, D.; Lou, S.; Wu, Z.; Guo, S.; Jing, S.; Li, Y.; Huang, C.; Tyndall, G. S.; Orlando, J. J.; Zhang, X. Atmospheric Processing of Nitrophenols and Nitrocresols From Biomass Burning Emissions. *Journal of Geophysical Research: Atmospheres* **2020**, *125* (22), e2020JD033401. https://doi.org/10.1029/2020JD033401.
(58) Kortüm, G.; Vogel, W.; Andrussow, K. Disssociation Constants of Organic Acids in Aqueous Solution. *Pure and Applied Chemistry* **1960**, *1* (2–3), 187–536. https://doi.org/10.1351/pac196001020187.
(59) Zhao, H.; Jiang, X.; Han, D.; Sun, Y.; Liu, Y.; Song, X.; Sheng, X. Revealing the Role of Metals and Anions in Nitrophenol UV–Visible Spectroscopies and Their Atmospheric Implication. *ACS Earth and Space Chemistry* **2021**. https://doi.org/10.1021/acsearthspacechem.1c00117.
(60) Lüttke, J.; Scheer, V.; Levsen, K.; Wünsch, G.; Neil Cape, J.; Hargreaves, K. J.; Storeton-West, R. L.; Acker, K.; Wieprecht, W.; Jones, B. Occurrence and Formation of Nitrated Phenols in and out of Cloud. *Atmospheric Environment* **1997**, *31* (16), 2637–2648. https://doi.org/10.1016/S1352-2310(96)00229-4.
(61) Harrison, M. A. J.; Barra, S.; Borghesi, D.; Vione, D.; Arsene, C.; Iulian Olariu, R. Nitrated Phenols in the Atmosphere: A Review. *Atmospheric Environment* **2005**, *39* (2), 231–248. https://doi.org/10.1016/j.atmosenv.2004.09.044.
(62) Kaur Kohli, R.; Van Berkel, G. J.; Davies, J. F. An Open Port Sampling Interface for the Chemical Characterization of Levitated Microparticles. *Anal. Chem.* **2022**, *94* (8), 3441–3445. https://doi.org/10.1021/acs.analchem.1c05550.
(63) Forrister, H.; Liu, J.; Scheuer, E.; Dibb, J.; Ziemba, L.; Thornhill, K. L.; Anderson, B.; Diskin, G.; Perring, A. E.; Schwarz, J. P.; Campuzano-Jost, P.; Day, D. A.; Palm, B. B.; Jimenez, J. L.; Nenes, A.; Weber, R. J. Evolution of Brown Carbon in Wildfire Plumes. *Geophysical Research Letters* **2015**, *42* (11), 4623–4630. https://doi.org/10.1002/2015GL063897.
(64) Dalton, A. B.; Nizkorodov, S. A. Photochemical Degradation of 4-Nitrocatechol and 2,4-Dinitrophenol in a Sugar-Glass Secondary Organic Aerosol Surrogate. *Environ. Sci. Technol.* **2021**, *55* (21), 14586–14594. https://doi.org/10.1021/acs.est.1c04975.